Raman Spectroscopy Study of Lattice Vibration and Crystallographic Orientation of Monolayer MoS_2 under Uniaxial Strain

*Yanlong Wang, Chunxiao Cong, Caiyu Qiu, and Ting Yu**

Molybdenum disulfide (MoS_2), a typical candidate of transition metal dichalcogenides (TMDs) with layered structure is emerging as one of the most promising materials. In particular, atomic thin layers of MoS_2 are believed to be the potential alternatives to graphene due to their advantage of the as-born bandgap, which is perfectly appropriate for optoelectronics. An indirect bandgap for thick MoS_2 layers (*i.e.* $n \geq 2$) becomes a direct bandgap of 1.8 eV in monolayer MoS_2,[1,2] consisting of two sulfide atomic layers and a layer of sandwiched Mo atoms.[3] The bandgap of monolayer MoS_2 could be further tuned by applying strain.[4–6] Therefore, its nature of being ultrathin transparent semiconductor offers a promising future to monolayer MoS_2 for applications of optoelectronics and energy harvesting. Most recently, monolayer MoS_2 field-effect transistors (FETs) have demonstrated a field-effect mobility of 320 $cm^2V^{-1}s^{-1}$, which is comparable to silicon, and a high current on/off ratio of 10^8.[7,8]

Raman spectroscopy has been widely used to study graphene, for example to probe the number of layers,[9] the stacking sequences,[10,11] the edge orientations,[12–14] the molecular doping,[15] the strain effects,[16–18] and the crystallographic orientation.[19,20] Since MoS_2 layers are structurally like graphene layers, similar Raman studies performed on graphene layers have been performed for the research of MoS_2 layers recently, such as identifying the number of layers,[21,22] investigating the electrical doping effects,[23] and the thermal effects.[24] In this work, we perform micro-Raman spectroscopy measurements of monolayer MoS_2 on flexible substrate, polyethylene terephthalate (PET), under controllable uniaxial tensile strain. Our observations reveal that the obvious red-shift of $E_{2g}{}^1$ mode with increasing strain can be used for monitoring the amount of strain. And the polarization response of the two splitted subbands, $E_{2g}{}^{1+}$ and $E_{2g}{}^{1-}$, is an effective indicator of the crystallographic orientation of monolayer MoS_2.

Bulk MoS_2 belongs to the $D_{6h}{}^4$ space group and possesses 12 lattice vibration modes at the Γ point.[25,26] Four of them are first-order Raman-active modes, named by their symmetries as E_{1g} (286 cm^{-1}), $E_{2g}{}^1$ (383 cm^{-1}), A_{1g} (408 cm^{-1}) and $E_{2g}{}^2$ (32 cm^{-1}).[27,28] In a backscattering configuration with laser beam propagating along the *c*-axis of MoS_2 crystal (adopted in this work), E_{1g} mode is forbidden while A_{1g} and E_{2g} are allowed.[25,26] In this work, the monolayer MoS_2 was identified by reading positions and/or the difference of the positions of $E_{2g}{}^1$ and A_{1g} modes, which is a widely adopted way to identify the number of layers of thin MoS_2 flakes,[21,22,29] and further verified by photoluminescence (PL) spectroscopy (see Figure S1). **Figure 1**(a) presents the typical Raman spectrum of monolayer MoS_2 on PET in the range of 200 cm^{-1} to 1150 cm^{-1}. Two dominant peaks locating at 384 cm^{-1} and 403 cm^{-1}, correspond to the $E_{2g}{}^1$ and A_{1g} modes, respectively. The deviations of the frequencies of these two modes from bulk to monolayer, for example, red shifting of 5 cm^{-1} for A_{1g} mode and blue shifting of 1 cm^{-1} for $E_{2g}{}^1$ mode, are mainly due to the decrease of the force constant resulted from the weakening of the interlayer Van der Waals force in MoS_2 layers (for A_{1g} mode) and the structure changes or long-range Coulombic interlayer interactions (for $E_{2g}{}^1$ mode) when the number of layers decreases.[29] In addition to the strong $E_{2g}{}^1$ and A_{1g} modes, we also observed peaks of MoS_2 at 447 cm^{-1}, 564 cm^{-1}, 593 cm^{-1} and 750 cm^{-1}, which could be assigned as $2LA(M)$, $2E_{1g}$, $E_{2g}{}^1+LA(M)$ and $2E_{2g}{}^1$ modes, respectively.[27,30] To further identify the crystallographic orientation of monolayer MoS_2 by probing polar behaviour of $E_{2g}{}^1$ and A_{1g} modes under uniaxial strain, we performed polarization dependent Raman measurements of the pristine monolayer MoS_2 without strain. As shown in Figure 1(b), the A_{1g} mode exhibits remarkable polar dependence and almost cannot be detected when the polarizations of the incident light and scattered light are orthogonal, while the intensities of the $E_{2g}{}^1$ mode vary very slightly. Our fitting results (Figure 1(c)) further clearly reveal the nature of polar behaviour of these two modes, which could be perfectly explained by the Raman selection rules as given by their Raman tensors (more discussion in SI).

Y. L. Wang, Dr. C. X. Cong, Dr. C. Y. Qiu, Prof. T. Yu
Division of Physics and Applied Physics
School of Physical and Mathematical Sciences
Nanyang Technological University
637371 Singapore
E-mail: yuting@ntu.edu.sg
Prof. T. Yu
Department of Physics
Faculty of Science
National University of Singapore
117542 Singapore, Graphene Research Centre
National University of Singapore
117546 Singapore

DOI: 10.1002/smll.201202876

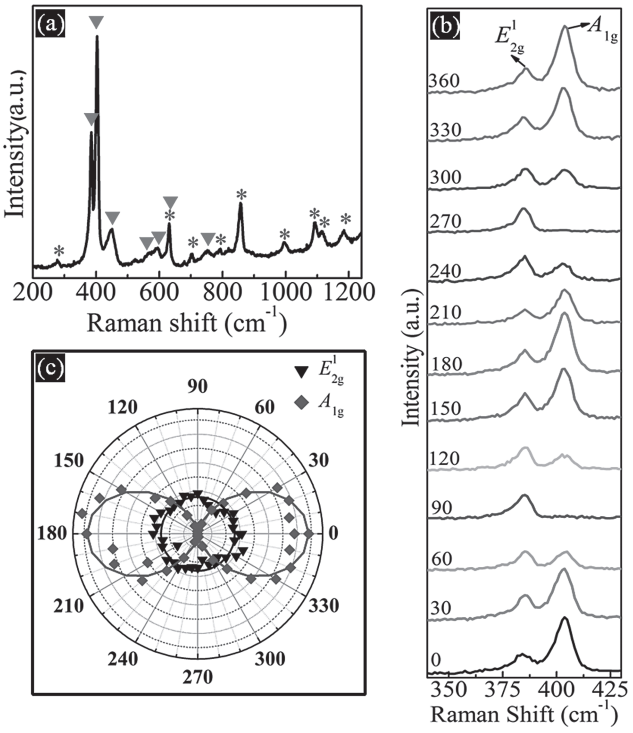

Figure 1. (a) Typical Raman spectrum of monolayer MoS_2 on PET. The Raman peaks labeled by ▾ are vibration modes of monolayer MoS_2, which are $E_{2g}{}^1$ (384 cm^{-1}), A_{1g} (403 cm^{-1}), $2LA(M)$ (447 cm^{-1}), $2E_{1g}$ (564 cm^{-1}), $E_{2g}{}^1 + LA(M)$ (593 cm^{-1}), and $2E_{2g}{}^1$ (750 cm^{-1}). Raman peaks marked by * are from PET. (b) Raman spectra of $E_{2g}{}^1$ and A_{1g} modes of the as-prepared monolayer MoS_2 on a PET substrate as a function of the angle between the polarizations of the incident and the scattered lights. (c) Polar plot of the fitted intensities of $E_{2g}{}^1$ and A_{1g} modes as a function of angles between the polarizations of the incident and scattered lights.

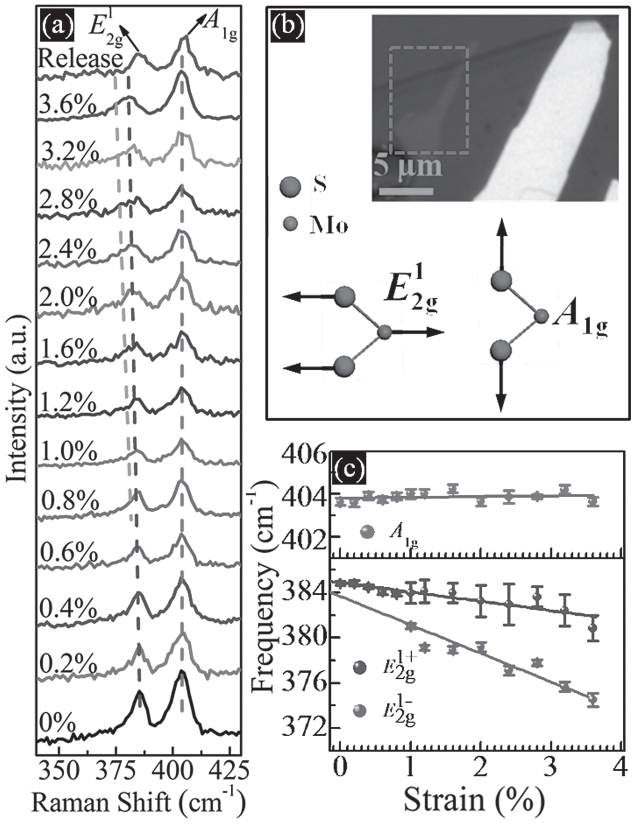

Figure 2. (a) Evolution of the Raman spectra of $E_{2g}{}^1$ and A_{1g} modes of the monolayer MoS_2 on PET substrate under uniaxial strain. The dash lines are the guide of the peak centers. (b) Optical image of the monolayer MoS_2 (highlighted by red dash line) on PET and the schematic diagram of the vibration of the $E_{2g}{}^1$ and A_{1g} modes. (c) Vibration frequencies of $E_{2g}{}^1$ and A_{1g} modes as a function of the uniaxial strain. The solid lines are the linear fits. $E_{2g}{}^1$ mode splits into two sub-peaks when strain is beyond 1%.

Figure 2(a) shows Raman spectra of $E_{2g}{}^1$ and A_{1g} modes of monolayer MoS_2 as a function of the uniaxial strain. While the frequencies of A_{1g} mode keep unchanged, an obvious red-shift occurs to $E_{2g}{}^1$ mode with increasing strain. This pristinely doubly degenerate optical phonon mode ($E_{2g}{}^1$) further splits into two singlet sub-bands, named $E_{2g}{}^{1+}$ and $E_{2g}{}^{1-}$, according to their energies, when the strain is more than 1%, and the original symmetry is lowered by strain. As shown in Figure 2(b), the $E_{2g}{}^1$ mode involves opposite vibration of two S atoms with respect to the Mo atom in the basal plane while the A_{1g} mode results from the vertical or out-of-plane vibration of only S atoms in opposite directions.[29] Our experimental findings clearly indicate that the dominated covalent bonding between Mo and S atoms is fairly sensitive to the in-plane uniaxial strain, which could indirectly evidence the change of the electronic properties of monolayer MoS_2 through the strain induced change in projected orbitals energy of Mo and the coupling between the Mo atom *d* orbital and the S atom *p* orbital.[4,6] Figure 2(c) plots the peak positions of the A_{1g}, $E_{2g}{}^{1+}$ and $E_{2g}{}^{1-}$ modes fitted by Lorentz lines. The Raman spectra of monolayer MoS_2 under strain of 0%, 1.0%, 2.4% and 3.6% were plotted together with fitted curves in Figure S3 to detail the evolution of of $E_{2g}{}^1$ and A_{1g} modes under uniaxial strain. We fitted the $E_{2g}{}^1$ Raman peak with strain of <1.0% and ≥1.0% by single Lorentz and two Lorentz peaks, respectively, because the $E_{2g}{}^1$mode starts to split into two singlet sub-bands at strain of 1.0%. The linear fittings of the $E_{2g}{}^{1+}$ and $E_{2g}{}^{1-}$ modes demonstrate their shift rates of (–0.8 ± 0.1) cm^{-1}/% and (–2.5 ± 0.3) cm^{-1}/%, respectively, which are much smaller than those of graphene.[20] To further understand the uniaxial strain effects on the $E_{2g}{}^1$ mode, the Grüneisen parameter ($\gamma_{E^1_{2g}}$) and the shear deformation potential ($\beta_{E^1_{2g}}$) are calculated by the simplified equations (see detailed discussion in SI):[20]

$$\gamma_{E^1_{2g}} = -\frac{P_{E^{1+}_{2g}} + P_{E^{1-}_{2g}}}{2\omega^o_{E^1_{2g}}(1-v)} \quad (1)$$

$$\beta_{E^1_{2g}} = \frac{P_{E^{1+}_{2g}} - P_{E^{1-}_{2g}}}{\omega^o_{E^1_{2g}}(1+v)} \quad (2)$$

where $P_{E^1_{2g}}$ is the shift rate, $\omega^0_{E^1_{2g}}$ is the original (zero-strain) frequency of $E_{2g}{}^1$, and v = 0.33 is the Poisson factor of the flexible substrate (PET in this work). From the Equation (1) and (2) and the data in Figure 2(c), $\gamma_{E^1_{2g}}$ and $\beta_{E^1_{2g}}$ of monolayer MoS_2 are 0.6 and 0.3, respectively, which are also smaller than those of graphene.[20]

NANO MICRO small

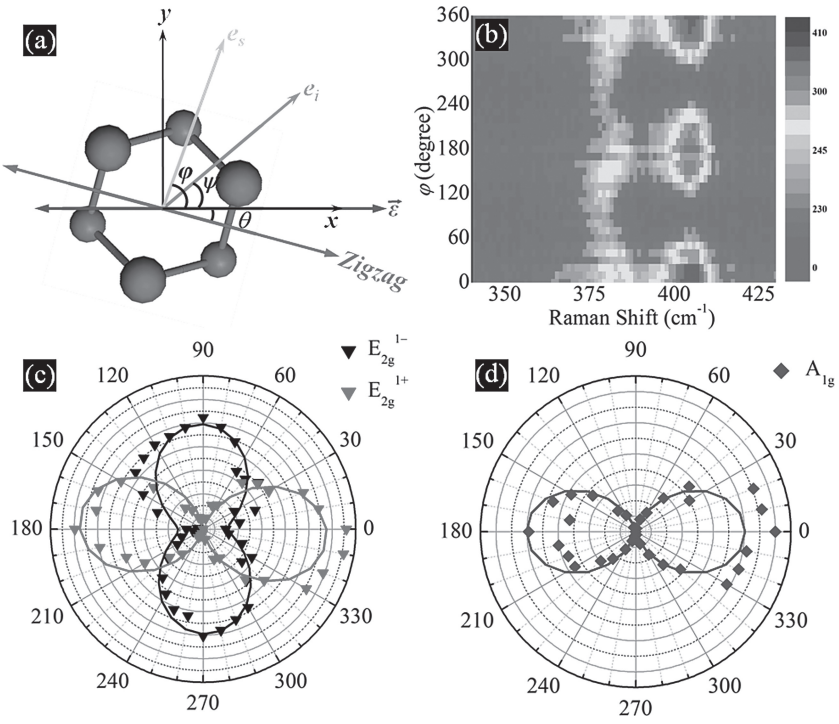

Figure 3. (a) Schematic diagram of the configuration of our polar-Raman measurements. $\vec{\varepsilon}$ is the strain direction which is fixed along to the horizontal direction (*x*-axis) and with an angle of θ to the zigzag direction of crystal lattice. e_i and e_s indicate the polarization of the incident and scattered lights, which deviate from the direction of strain by angles of ψ and ϕ, respectively. (b) False-color image of the intensity of Raman spectra as a function of the relative Raman shift and the angle ϕ under uniaxial strain of 3.6%. (c) and (d) are polar plots of the fitted peak intensities of E_{2g}^{1+}, E_{2g}^{1-} and A_{1g} modes as a function of angle ϕ.

Polarization dependent Raman spectroscopy has been used to study the crystallographic orientation of graphene.[19,20] In this work, we employed this technique to identify the crystallographic orientation of monolayer MoS_2. **Figure 3**(a) illustrates the configuration of our polar-Raman measurements. We fixed the strain direction along the horizontal direction (*x*-axis) and aligned the polarization of the incident laser coincidently, meaning angle $\psi = 0^o$. The polarization of the scattered light with respect to the strain direction or the angle ϕ is tuned by rotating an analyzer. By this way, we are able to obtain the Raman spectra of the monolayer MoS_2 under uniaxial strain of 3.6% as a function of polar angle ϕ (see Figure S4) and plot the false-color (3D type) image of the intensity of the spectra versus both peak positions and polar angles (see Figure 3(b)). It is noticed that the strongest E_{2g}^{1+} and E_{2g}^{1-} peaks appear at different angles, reflected as the alternation of the maxima of the intensity within the frequency range of the E_{2g}^{1} mode while the minima and maxima of the A_{1g} mode present in the same line of the relative Raman shift. To further understand the polar behaviors of the E_{2g}^{1+}, E_{2g}^{1-} and A_{1g} modes under a uniaxial strain and consequently identify the crystallographic orientation of monolayer MoS_2, we performed the Lorentz fitting and plotted the fitted intensities of these three modes as a function of the polar angle ϕ in 2D polar maps (Figure 3(c) and (d)). The same as under zero-strain, A_{1g} mode follows a $cos^2\phi$ dependence as it is very insensitive to in-plane uniaxial strain. In very contrast to the non-polar dependence of the E_{2g}^{1} mode for the unstrained monolayer MoS_2 (Figure 1(c)), the splitted E_{2g}^{1+} and E_{2g}^{1-} modes induced by uniaxial strain are extremely sensitive to the polarization. For example, the E_{2g}^{1+} mode almost vanishes when the polarization of the scattered light is perpendicular to that of the incident laser, also to the strain axis ($\phi = 90^o$), while the E_{2g}^{1-} mode is the strongest. Further rotating the analyzer by 90 degrees ($\phi = 180^o$), one can find the maximum of the E_{2g}^{1+} and the minimum of the E_{2g}^{1-}. This indicates that the linear polarizations of the scattered light from E_{2g}^{1+} and E_{2g}^{1-} are orthogonal.

The splitting of E_{2g}^{1} mode into two modes is induced by applying uniaxial strain and consequently changing the crystal structure or symmetry. Thus, the intensities of the polarized scattered light from these two modes are dependent on the direction of the strain with respect to the crystal lattice as predicted by the equations (see the derivation in SI):[19,20]

$$I_{E_{2g}^{1+}} \propto d^2 \cos^2(\phi + \psi + 3\theta) \quad (3)$$

$$I_{E_{2g}^{1-}} \propto d^2 \sin^2(\phi + \psi + 3\theta) \quad (4)$$

here ψ is zero as we fixed the polarization of the incident laser and the strain axis in the same direction. The good agreement between the experimental data and the fittings (by Equation (3) and (4)) firmly supports the theoretical analysis and the value of θ reveals the crystal lattice orientation. For the sample shown in Figure 2(b) inset, the zigzag direction accidentally happens to be very close to the strain axis.

To further confirm the above analysis, we conducted polar-Raman on another piece of monolayer MoS_2 on PET under uniaxial strain of 2.8%, which is sufficient to split the E_{2g}^{1} mode into two sub-bands. Consistently, the A_{1g} mode follows the function of a cosine square perfectly (see Figure S5), and the polarizations of the scattered light from E_{2g}^{1+} and E_{2g}^{1-} are linear and orthogonal. Now, according to the previous discussion, if we change the angle between the crystal lattice, *i.e.* zigzag direction and the strain direction (fixed along *x*-axis), we should observe different polarization response of both E_{2g}^{1+} and E_{2g}^{1-} modes. We re-mounted the same sample including the PET substrate and the same piece of monolayer MoS_2 by rotating an angle of ~90° relevant to the *x*-axis after fully released the strain, monitored by reading the position of E_{2g}^{1} mode. As suspected, the E_{2g}^{1+} and E_{2g}^{1-} modes behave differently to the polar angles and the maxima as well as minima of both two modes shifted, which confirms the previous theory and our experimental

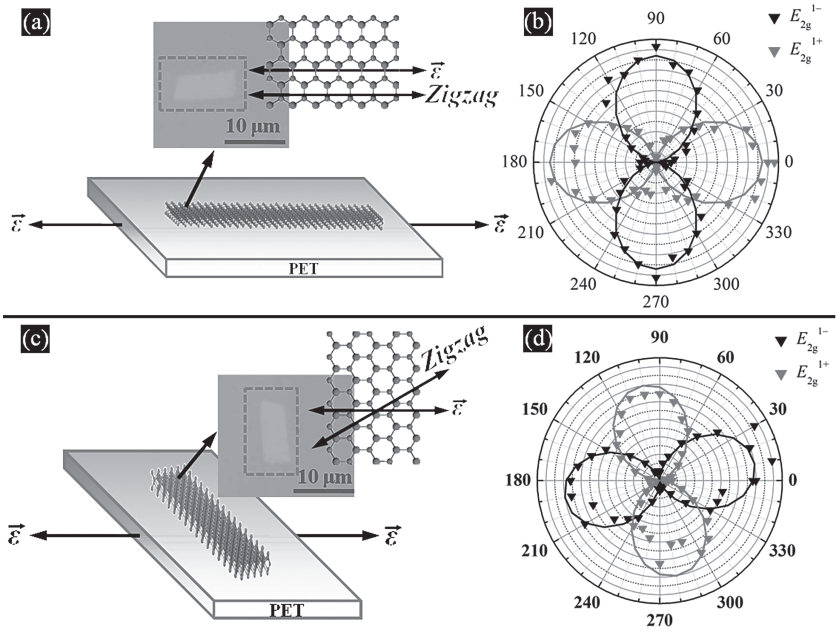

Figure 4. (a) and (c) Schematic diagrams and optical images of the same piece of monolayer MoS_2 on PET by applying uniaxial strain along different directions. (b) and (d) Polar plots of the fitted peak intensities of $E_{2g}{}^{1+}$, and $E_{2g}{}^{1-}$ modes as a function of angle ϕ. Note: for (c) and (d) the sample including both PET and monolayer MoS_2 flake was remounted by rotating ~90º with respect to the fixed strain axis after fully releasing the strain.

findings. The data in **Figure 4**(b) and (d) are well fitted by $I_{E_{2g}^{1+}} \propto \cos^2(\varphi)$, $I_{E_{2g}^{1-}} \propto \sin^2(\varphi)$, and $I_{E_{2g}^{1+}} \propto \cos^2(\varphi + 80^\circ)$, $I_{E_{2g}^{1-}} \propto \sin^2(\varphi + 80^\circ)$, respectively. According to Equation (3) and (4), we get $\theta = 0^\circ$ (before re-mounted) and $\theta = 26.7^\circ$ (after re-mounted). This is coincident with the angle of ~90º the sample rotated, which makes the crystallographic orientation (zigzag direction) with respect to the known strain axis (θ) change from 0º to ~30º (The angle of 26.7 obtained by the polar-Raman measurement is very close to this value.).

In summary, we have successfully transferred monolayer MoS_2 on flexible substrate by mechanical exfoliation and conducted micro-Raman spectroscopy investigation of such 2D semiconductor flake under tunable uniaxial tensile strain. We find that the doubly degenerate $E_{2g}{}^1$ mode shows obvious red-shift when increasing strain and eventually splits into two modes, $E_{2g}{}^{1+}$ and $E_{2g}{}^{1-}$, when the strain is high enough to break the original lattice symmetry. The intensities of these two modes orthogonally respond to the angle between the polarization of the scattered light and the strain axis. Such polarization dependence could be adopted for determination of the crystallographic orientation of monolayer MoS_2. Our findings can be very meaningful for study of the mechanical and electronic properties of 2D MoS_2 and other transition metal dichalcogenides under strain.

Experimental Section

The MoS_2 samples were fabricated by micromechanical cleavage of a bulk MoS_2 (429ML-AB, molybdenum disulfide, single crystals from USA, SPI Supplies) and then transferred onto PET substrates.

The Raman and PL spectra were obtained using a WITec CRM200 Raman system with 1800 and 150 lines/mm grating respectively with 532 nm excitation laser. The laser spot is about 0.5 μm in diameter. Laser power at the sample was carefully controlled to avoid laser-induced heating. A 100x objective lens with a numerical aperture (N.A.) of 0.95 was used in both Raman and PL experiments.

Supporting Information

Supporting Information is available from the Wiley Online Library or from the author.

Acknowledgements

Y. L. Wang and C. X. Cong contributed equally to this work. This work is supported by the Singapore National Research Foundation under NRF RF Award No. NRFRF2010-07.

[1] K. Mak, C. Lee, J. Hone, J. Shan, T. Heinz, *Phys. Rev. Lett.* **2010**, *105*, 136805.
[2] A. Splendiani, L. Sun, Y. Zhang, T. Li, J. Kim, C.-Y. Chim, G. Galli, F. Wang, *Nano Lett.* **2010**, *10*, 1271.
[3] G. Lucovsky, R. White, J. Benda, J. Revelli, *Phys. Rev. B* **1973**, *7*, 3859.
[4] P. Lu, X. Wu, W. Guo, X. C. Zeng, *Phys. Chem. Chem. Phys.* **2012**, *14*, 13035.
[5] E. Scalise, M. Houssa, G. Pourtois, V. Afanas'ev, A. Stesmans, *Nano Res.* **2011**, *5*, 43.
[6] P. Johari, V. B. Shenoy, *ACS Nano* **2012**, *6*, 5449.
[7] B. Radisavljevic, M. B. Whitwick, A. Kis, *ACS Nano* **2011**, *5*, 9934.
[8] B. Radisavljevic, J. Brivio, V. Giacometti, A. Kis, A. Radenovic, *Nat. Nanotechnol.* **2011**, *6*, 147.
[9] A. C. Ferrari, J. C. Meyer, V. Scardaci, C. Casiraghi, M. Lazzeri, F. Mauri, S. Piscanec, D. Jiang, K. S. Novoselov, S. Roth, A. K. Geim, *Phys. Rev. Lett.* **2006**, *97*, 187401.
[10] C. X. Cong, T. Yu, R. Saito, G. F. Dresselhaus, M. S. Dresselhaus, *ACS Nano* **2011**, *5*, 1600.
[11] C. X. Cong, T. Yu, K. Sato, J. Z. Shang, R. Saito, G. F. Dresselhaus, M. S. Dresselhaus, *ACS Nano* **2011**, *5*, 8760.
[12] C. Casiraghi, A. Hartschuh, H. Qian, S. Piscanec, C. Georgi, A. Fasoli, K. S. Novoselov, D. M. Basko, A. C. Ferrari, *Nano Lett.* **2009**, *9*, 1433.
[13] Y. M. You, Z. H. Ni, T. Yu, Z. X. Shen, *Appl. Phys. Lett.* **2008**, *93*, 163112.
[14] C. X. Cong, T. Yu, H. M. Wang, *ACS Nano* **2010**, *4*, 3175.
[15] N. Peimyoo, J. Li, J. Shang, X. Shen, C. Qiu, L. Xie, W. Huang, T. Yu, *ACS Nano* **2012**, *6*, 8878.
[16] T. Yu, Z. H. Ni, C. L. Du, Y. M. You, Y. Y. Wang, Z. X. Shen, *J. Phys. Chem. C* **2008**, *112*, 12602.
[17] Z. H. Ni, T. Yu, Y. H. Lu, Y. Y. Wang, Y. P. Feng, Z. X. Shen, *ACS Nano* **2008**, *2*, 2301.
[18] D. Yoon, Y.-W. Son, H. Cheong, *Phys. Rev. Lett.* **2011**, *106*, 155502.

[19] M. Huang, H. Yan, C. Chen, D. Song, T. F. Heinz, J. Hone, *Proc Natl Acad Sci USA* **2009**, *106*, 7304.
[20] T. Mohiuddin, A. Lombardo, R. Nair, A. Bonetti, G. Savini, R. Jalil, N. Bonini, D. Basko, C. Galiotis, N. Marzari, K. Novoselov, A. Geim, A. Ferrari, *Phys. Rev. B* **2009**, *79*, 205433.
[21] C. Lee, H. Yan, L. E. Brus, T. F. Heinz, J. Hone, S. Ryu, *ACS Nano* **2010**, *4*, 2695.
[22] A. Molina-Sánchez, L. Wirtz, *Phys. Rev. B* **2011**, *84*, 155413.
[23] B. Chakraborty, A. Bera, D. V. S. Muthu, S. Bhowmick, U. V. Waghmare, A. K. Sood, *Phys. Rev. B* **2012**, *85*, 161403.
[24] S. Najmaei, Z. Liu, P. M. Ajayan, J. Lou, *Appl. Phys. Lett.* **2012**, *100*, 013106.
[25] T. Sekine, T. Nakashizu, K. Toyoda, K. Uchinokura, E. Matsuura, *Solid State Commun.* **1980**, *35*, 371.
[26] T. J. Wieting, J. L. Verble, *Phys. Rev. B* **1971**, *3*, 4286.
[27] J. M. Chen, C. S. Wang, *Solid State Commun.* **1974**, *14*, 857.
[28] C. Sourisseau, M. Fouassier, M. Alba, A. Ghorayeb, O. Gorochov, *Mater. Sci. Eng. B* **1989**, *3*, 119.
[29] H. Li, Q. Zhang, C. C. R. Yap, B. K. Tay, T. H. T. Edwin, A. Olivier, D. Baillargeat, *Adv. Funct. Mater.* **2012**, *22*, 1385.
[30] G. L. Frey, R. Tenne, M. J. Matthews, M. S. Dresselhaus, G. Dresselhaus, *Phys. Rev. B* **1999**, *60*, 2883.

Received: November 19, 2012
Revised: January 15, 2013
Published online: April 22, 2013

